Phase Stability Control of Interstitial Oxide Ion Conductivity in the La$_{1+x}$Sr$_{1-x}$Ga$_3$O$_{7+x/2}$ Melilite Family

Chris I. Thomas, Xiaojun Kuang, Zengqiang Deng, Hongjun Niu, John B. Claridge, and Matthew J. Rosseinsky*

Department of Chemistry, University of Liverpool, Liverpool, L69 7ZD, U.K.

Received October 10, 2009. Revised Manuscript Received February 13, 2010

The two-dimensional polyhedral anion network melilites La$_{1+x}$Sr$_{1-x}$Ga$_3$O$_{7+0.5x}$ exhibit interstitial oxide ion conductivity. The solid solution is shown to extend to $x = 0.64$, and the variation of the conductivity with x is investigated. At high temperatures, all of these compounds adopt the typical tetragonal melilite structure. When $x > 0.6$, cooling below 600 °C results in a reversible phase transition to an orthorhombic structure which reduces the ionic conductivity. Quenching experiments have shown the tetragonal structure has a higher conductivity compared to the orthorhombic structure of the same composition. Short-range order effects associated with this transition exercise an important influence on the composition- and temperature-dependence of the conductivity.

Introduction

Solid oxide fuel cells (SOFCs) have particular advantages over other types of fuel cells such as modularity and fuel flexibility[1] with the ability to use a range of fuels from high purity H$_2$ to readily available hydrocarbons.[2] However current SOFCs require high temperatures, e.g., above 700 °C, for Yttria stabilized zirconia (YSZ)[3] or above 500 °C for gadolinium doped cerium oxide (CGO)[4] systems for operation. At these temperatures, the ions become mobile enough for efficient operation of the cell, but the thermal expansion and reactivity of the fuel cell components becomes problematic.[5] For SOFCs to become competitive with current technology, oxide ion electrolytes with specific conductivities exceeding 10^{-2} S/cm at low (~500 °C) temperatures are required,[6] motivating the search for materials displaying new combinations of carrier and structure type.

Recently, the two-dimensional complex anion network melilites[7,8] La$_{1+x}$Sr$_{1-x}$Ga$_3$O$_{7+0.5x}$ have been shown to exhibit interstitial[9] oxide ion conduction of 0.02–0.1 S/cm at $x = 0.54$ over the 600–900 °C temperature range, this is unusual, as interstitials are usually found in isolated anions rather than network structures. Rozumek and co-workers[7,8] present data from $x = -0.15$ to 0.60, while Kuang and co-workers[9] suggest that $x = 0.6$ is the maximum value of x which will retain the parent structure with disordered oxide ion interstitials. The $x = 0$ parent material LaSrGa$_3$O$_7$ is tetragonal (T) ($a_{\text{tetra}} = 8.056$ Å, $c_{\text{tetra}} = 5.333$ Å[10] (Figure 1)). La and Sr occupy the eight coordinate A site while the smaller Ga occupies two distinct tetrahedral sites (3-connected, with a nonbridging terminal oxide, and 4-connected with all oxides bridging to neighboring tetrahedra) in a corner-shared tetrahedral 2D layer with a distorted pentagonal tunnel which is occupied by the interstitial oxygen charge carriers required for charge balance when $x > 0$. Above and below the center of each tunnel are the A sites (Figure 1). This paper addresses the limits on the extent of La substitution for Sr in single-phase materials and thus on the interstitial anion carrier density and ionic conductivity. The highest carrier concentrations produce long-range static structural ordering of the interstitials which strongly influences the ionic transport.

Experimental Section

Synthesis and Processing. Phase relations of La$_2$O$_3$–SrO–Ga$_2$O$_3$ in the La$_{1+x}$Sr$_{1-x}$Ga$_3$O$_{7+0.5x}$ series were investigated by solid state reaction using La$_2$O$_3$ (99.999%, Alfa Aesar), SrCO$_3$ (99.995%, Aldrich), and Ga$_2$O$_3$ (99.999%, Alfa Aesar) as starting materials, which were mixed in ethanol and calcined at 1200 °C for 12 h. Due to La$_2$O$_3$ absorbing water and CO$_2$ at ambient temperatures, the La$_2$O$_3$ powder was stored in a furnace at 950 °C prior to weighing. After regrinding, the powders were uniaxially pressed into pellets, placed on platinum foil (99.95%, Goodfellow Ltd.), in covered alumina crucibles (Almath Crucibles Ltd. 99.8%) and fired at 1400 °C ($x = 0$–0.54) or 1350 °C ($x = 0.56$–0.64) for 12 h. To counter the

*Corresponding author. E-mail: rossein@liverpool.ac.uk.
(1) Eguchi, K.; Kikuchi, R.; Takeguchi, T. *Proc. Electrochem. Soc.* **2003**, *2002–2026*, 38–52.
(2) Minh, N. Q. *J. Am. Ceram. Soc.* **1993**, *76*, 563–588.
(3) Brett, D. J. L.; Atkinson, A.; Brandon, N. P.; Skinner, S. J. *Chem. Soc. Rev.* **2008**, *37*, 1568–1578.
(4) Steele, B. C. H. *Solid State Ionics.* **2000**, *129*, 95–110.
(5) Lashtabeg, A.; Skinner, S. J. *J. Mater. Chem.* **2006**, *16*, 3161–3170.
(6) Steele, B. C. H.; Heinzel, A. *Nature* **2001**, *414*, 345–352.
(7) Rozumek, M.; Majewski, P.; Schluckwerder, H.; Aldinger, F.; Kunstler, K.; Tomandl, G. *J. Am. Ceram. Soc.* **2004**, *87*, 1795–1798.
(8) Rozumek, M.; Majewski, P.; Sauter, L.; Aldinger, F. *J. Am. Ceram. Soc.* **2004**, *87*, 662–669.
(9) Kuang, X.; Green, M. A.; Niu, H.; Zajdel, P.; Dickinson, C.; Claridge, J. B.; Jantsky, L.; Rosseinsky, M. J. *Nat. Mater.* **2008**, *7*, 498–504.

(10) Steins, M.; Schmitz, W.; Uecker, R.; Doerschel, J. *Z. Kristallogr. - New Cryst. Struct.* **1997**, *212*, 76.
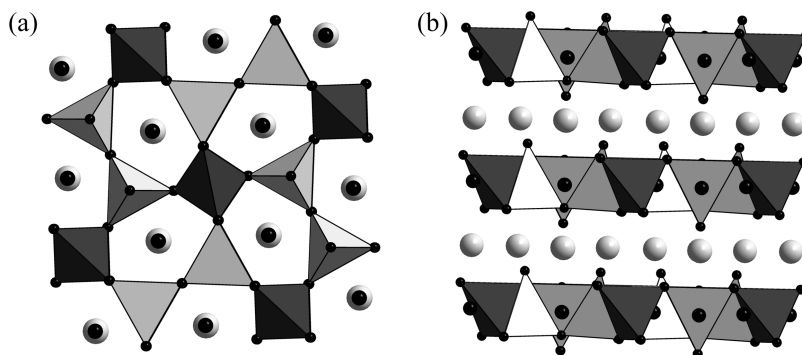
Figure 1. Melilite structure of $LaSrGa_3O_7$ showing the two types of GaO_4 tetrahedra (dark gray 4-connected, light gray/white 3-connected). Light gray spheres show the La/Sr sites, and the black spheres show oxygen. The spheres for the interstitial oxygen sites are larger than those for the framework oxygens. In part a, the view is down the *c* axis showing the Ga tetrahedra and the pentagonal tunnels. The view in part b along [110] shows that the interstitial oxygen sits in the center of the Ga layers with La/Sr cations above and below.

volatilization of Ga at high temperatures, a small excess was required meaning that instead of the 2:3 La/Sr:Ga ratio, this was 2:3.05 (1.7% excess Ga) for $x = 0.54-0.58$, 2:3.06 (2% excess Ga) for $x = 0.6$ and 0.62, and 2:3.07 (2.3% excess Ga) for $x = 0.64$. Postsynthesis XRD showed no evidence of Ga_2O_3 or other gallium rich impurities being present. If stoichiometric quantities or higher temperatures than stated above are used, a melilite phase is observed as the main phase but a perovskite phase is also visible in the powder XRD data.

Pellet samples with >90% of the theoretical density for electrical measurements were made via cold-isostatic pressing (CIP) with 206.85 MPa pressure after being calcined at 1200 °C for 12 h, followed by the final firing at 1350 °C for 12 h.

Quenching experiments were carried out by removing the alumina crucible from the furnace at 1350 °C and tipping the pellet out onto a block of aluminum at room temperature.

Characterization. The phase purity was checked by powder X-ray diffraction data with a Panalytical X'pert Pro Multi-Purpose X-ray diffractometer (Co $K\alpha_1$ radiation $\lambda = 1.78901$ Å) collected at ambient temperature. Silicon was added as an internal standard to refine the cell variation with composition. For the time-resolved study, a sample of metastable quenched T structured $La_{1.64}Sr_{0.36}Ga_3O_{7.32}$ in a 0.5 mm outside diameter amorphous fused silica capillary (Mark-Röhrchen quarzkapillaren) was measured at station I11 of the Diamond Light Source. Data were collected stepwise over $1.821-141.953\ 2\theta$ ($\lambda = 0.82545$ Å) in sequential 5 min data sets collected at 400 °C. Using the same wavelength, a separate capillary was heated from 300 to 600 °C. Also, 5 min data sets were collected over the same 2θ range in 5 °C steps with a ramp rate of 5 °C/min between scans. At 600 °C, a 20 min scan was taken of the sample at the end of the heating protocol.

Conductivity Measurement. Alternating current (ac) impedance spectroscopy (IS) measurements in air were performed with a Solartron 1255B Frequency Response Analyzer coupled to a Solartron 1287 electrochemical interface over the $10^{-2}-10^6$ Hz frequency range for measurements in the 350−980 °C range.

Pellets were prepared by first polishing both sides with silicon carbide paper, (Buehler P800 and P2500) then applying the electrodes. The electrodes used were made by painting the polished pellet with platinum paste (Metalor A4731) and firing at 150 °C for 1 h, then ramping to 300 °C holding for 1 h, then ramping to 800 °C holding for 1 h, and then ramping to 950 °C for the measurement. The ramp rate was set at 5 °C/min, and Engelhard CPPT platinum wire was used to connect the pellet to the Solartron leads.

For each sample, the pellet being measured was heated to 950 °C and left to dwell for an hour before the measurement took place. Measurements were then taken every 50 °C down to 350 °C with the measurement for each temperature only occurring after the sample had been left for 1 h at that temperature to ensure the sample had equilibrated.

The bulk and the grain boundary responses at higher frequencies overlap to exhibit part of an asymmetric semicircular arc. The intercept of the semicircular arc at low frequency was extracted as the total resistivity $R_b + R_{gb}$. Above 400 °C, the electrode response dominated the impedance data and gradually collapsed to a semicircular arc, giving two arcs in the impedance plot (Figure 2). The high frequency intercept of the second arc was taken as total resistivity $R_b + R_{gb}$ while the high frequency intercept of the first arc was taken as the bulk resistivity R_b. This allows the bulk and grain boundary resitivities to be separated over the region where the two arcs are visible (Supporting Information Figure S4). As the temperature is increased, the arc from the grain boundary response vanishes and only one semicircular arc from the electrode response was seen with the high frequency intercept being taken as the total resistivity $R_b + R_{gb}$.

Measurement of the conductivity of a quenched T sample of $La_{1.64}Sr_{0.36}Ga_3O_{7.32}$ on heating from 200 to 500 °C and subsequent cooling to 200 °C was performed to compare the conduction behaviors of tetragonal (T) and pseudo-orthorhombic phase (O) on materials with the same composition. The measurement was taken in 25 °C intervals over the entire temperature range with 1 h equilibration time at each temperature. For the quenched samples of $La_{1.64}Sr_{0.36}Ga_3O_{7.32}$, a Solartron 1296 dielectric interface was used instead of the Solartron 1287 electrochemical interface for measurements over the $10^{-2}-10^6$ Hz frequency range and the temperature range 200−500 °C on heating and cooling cycles. Instead of platinum electrodes, silver conductive paint which dries in air was used (Agar G3790) to allow for measurement to be carried out without the need to sinter electrodes at high temperatures. Note that at each temperature the samples dwell for 1 h, so the points for both cooling post 500 °C and for the furnace cooled sample will be single phase O. Further measurement on one more heating and cooling cycle from 200 to 500 °C after the conversion from the T phase to the O phase described in the text did not show significant change in the conductivity, suggesting that the O phase is stable to thermal cycling.

The ac conductivity as a function of partial pressure of oxygen (p_{O_2}) (monitored by a YSZ potentiometric sensor) was measured
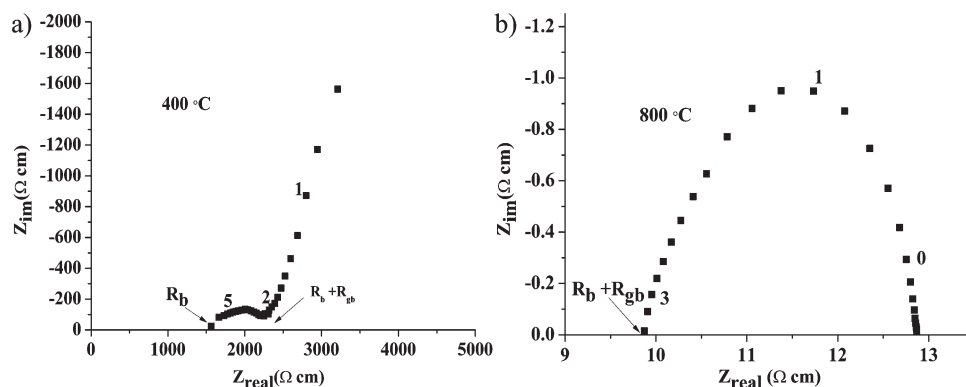
Figure 2. Complex impedance plots of $La_{1.6}Sr_{0.4}Ga_3O_{7.3}$ at 400 (a) and 800 °C (b). The numbers in bold on the plot indicate the frequency logarithms; the ac amplitude used for the measurements was 10 mV.

at 600 °C over a p_{O_2} range of $1-10^{-22}$ atm. The p_{O_2} value was controlled over $1-10^{-4}$ atm p_{O_2} range by dilution of O_2 with Ar, for $10^{-4}-10^{-22}$ atm by using mixed 1% CO in Ar and 1% CO_2 in Ar. The dwell time ranged from 5 to 24 h ($\sim$5$-$8 h for $p_{O_2} > 10^{-4}$ and 12$-$24 h for $p_{O_2} < 10^{-4}$) to allow equilibration of the samples with the gas environment at each point.

Diffuse Reflectance. The band gap of $LaSrGa_3O_7$ was measured on a polycrystalline sample using diffuse reflectance spectroscopy. Reflectance data were collected on a Perkin-Elmer LAMDA 650 S UV/vis spectrometer using $BaSO_4$ reflectance standards and converted to absorbance (using Kubelka$-$Munk). The band gap energy was then obtained by using the Shapiro method of extrapolating the onset of absorption to the wavelength axis.[11]

Infrared Spectroscopy (IR). The IR measurement was carried out on a Perkin-Elmer Spectrum 100 with ATR.

Thermogravimetric Analysis (TGA). The TGA measurement was carried out using a TA Instruments SDTQ600.

Energy-Dispersive X-ray Analysis (EDS). The EDS was carried out using a JEOL 2000FX transmission electron microscope operated at 200 kV.

Results

Ceramic synthesis with slight ($< 3\%$ depending on x, see the Experimental Section) excess Ga_2O_3 affords the $La_{1+x}Sr_{1-x}Ga_3O_{7+0.5x}$ ($x \leq 0.64$) samples studied here; $x = 0.65$ and 0.67 were also studied but did not afford single phases, instead forming a mixture of melilite and Sr-doped $LaGaO_3$ (LSG). The powder X-ray (XRPD) patterns (Figure 3) for $x < 0.6$ can be indexed using the T cell of the parent phase. However, for $x > 0.6$, the splitting of the $h, k \neq 0$ tetragonal reflections requires indexing with a pseudo-orthorhombic (O) cell ($a_{orth} \approx b_{orth} \sim \sqrt{2}a_{tetra}$, $c = c_{tetra}$). The true symmetry may be lower. The a parameter (Figure 4a) decreases linearly with x until the transition to the O structure, with the c parameter and the volume (Figure 4b) decreasing linearly across the entire composition range, accounted for by the smaller size of La^{3+}. $x = 0.64$ is the highest La content affording a single phase composition and is O at room temperature.
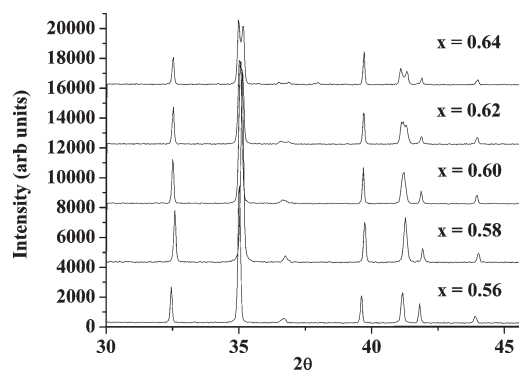
(11) Eng, H. W.; Barnes, P. W.; Auer, B. M.; Woodward, P. M. *J. Solid State Chem.* **2003**, *175*, 94–109.

Figure 3. XRD patterns of $La_{1+x}Sr_{1-x}Ga_3O_{7+x/2}$ ($x = 0.56. 0.58, 0.6, 0.62,$ and 0.64).

Variable temperature powder X-ray diffraction data for $La_{1.64}Sr_{0.36}Ga_3O_{7.32}$ (Supporting Information Figure S3) shows that the O to T transition takes place at 565 °C on heating. This transition can also be observed in the conductivity data as a change in the gradient (activation energy) of a $\ln(\sigma T)$ versus $1/T$ plot (Figure 8). An in situ PXRD scan at 600 °C was fitted using the LeBail method shown in Figure 5a showing that at 600 °C the pure T phase was observed. The transition from T to O is controlled by kinetic factors, demonstrated by furnace-cooled samples with $x > 0.6$ showing the presence of both phases (Figure 5b).

Pure T $La_{1.64}Sr_{0.36}Ga_3O_{7.32}$ can be prepared by quenching to room temperature from the high temperature T phase stability region at 1350 °C, with the mixed O and T phases accessed by furnace cooling at 15 °C/min. The pure O phase is produced by annealing either quenched T or furnace cooled T/O samples for 12 h at 400 °C. In-situ PXRD data at 400 °C revealed that the $h, k \neq 0$ single reflections of the quenched metastable T phase broadened and split completely within 30 min to obtain the single phase stable O structure (Figure 6a).

The synthesized samples are stable to 800 °C in air (Figure 6b). For $x \geq 0.4$, prolonged annealing above this temperature (for periods longer than the impedance measurements described later- all materials reported were examined by XRD postmeasurement to ensure their single phase nature was retained) causes the melilite to
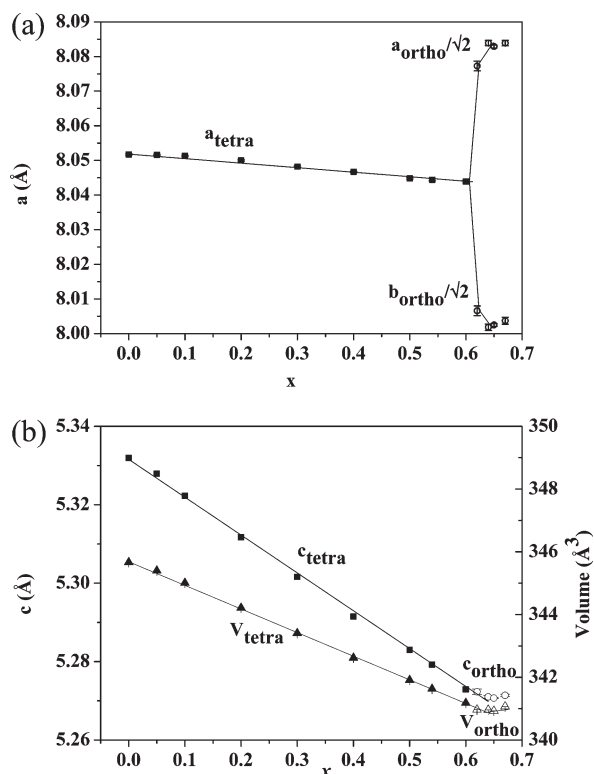
(a)

(b)

Figure 4. (a) a and b lattice parameters. (b) c parameter and unit cell volume of $La_{1+x}Sr_{1-x}Ga_3O_{7+x/2}$, $x = 0-0.67$. Data for $x < 0.6$ are from ref 9; that for $x > 0.6$ is from this work.

partially decompose with formation of the Sr-doped LSG perovskite (Figure 6b, black star) and Ga_2O_3 as detailed in the Supporting Information (SI) Figures S9 and S10, rendering conductivity comparisons with $La_{0.8}Sr_{0.2}Ga_{0.83}Mg_{0.17}O_{2.815}$ (LSGM) only meaningful below 800 °C at these higher doping levels. The instability with respect to LSG only occurs over a limited temperature range-reheating the phase separated mixture at 1350 °C affords the initial melilite, suggesting a complex sequence of phase stability (Figure S11).

Impedance data from the $La_{1+x}Sr_{1-x}Ga_3O_{7+0.5x}$ materials (Figures 2a and b) at < 400 °C exhibit a significant Warburg electrode[12,13] response with an associated large capacitance ($> 10^{-7}$ F cm^{-1}) in the low frequency range (< 10 Hz), which is characteristic of ionic conduction with partially blocking electrodes. The total conductivity of $La_{1.64}Sr_{0.36}Ga_3O_{7.32}$ at 600 °C is independent of oxygen partial pressure over the $1-10^{-22}$ atm range (Figure 7), as found earlier for $La_{1.54}Sr_{0.46}Ga_3O_{7.27}$[9] showing that there is pure ionic conductivity across the entire series $La_{1+x}Sr_{1-x}Ga_3O_{7+x/2}$ to the solid solution limit $x = 0.64$. Postmeasurement XRD of $La_{1.64}Sr_{0.36}Ga_3O_{7.32}$ (SI Figure S12) shows that the sample remains single phase.

The band gap of $LaSrGa_3O_7$ (measured by diffuse reflectance in SI Figure S7) is 5.0 eV, consistent with the absence of an intrinsic electronic contribution over the entire temperature range measured.
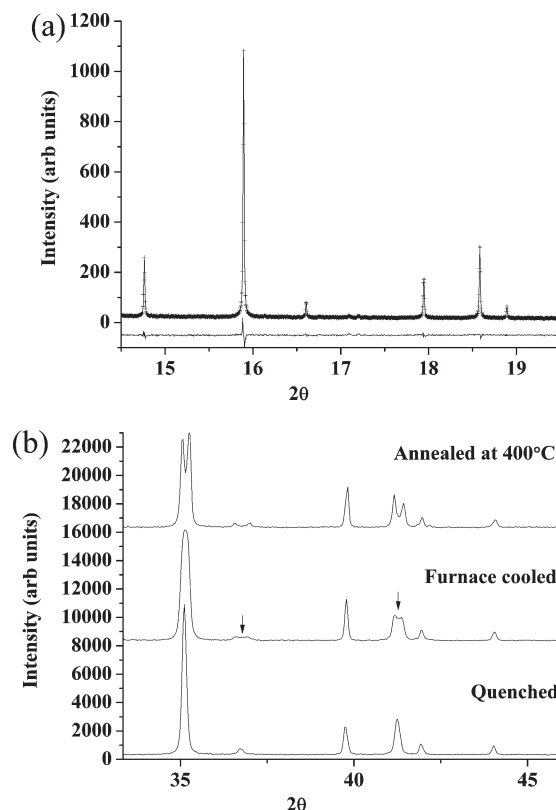
(12) Macdonald, J. R. *Impedance Spectroscopy Emphasizing solid materials and systems*; Wiley: New York, 1987.
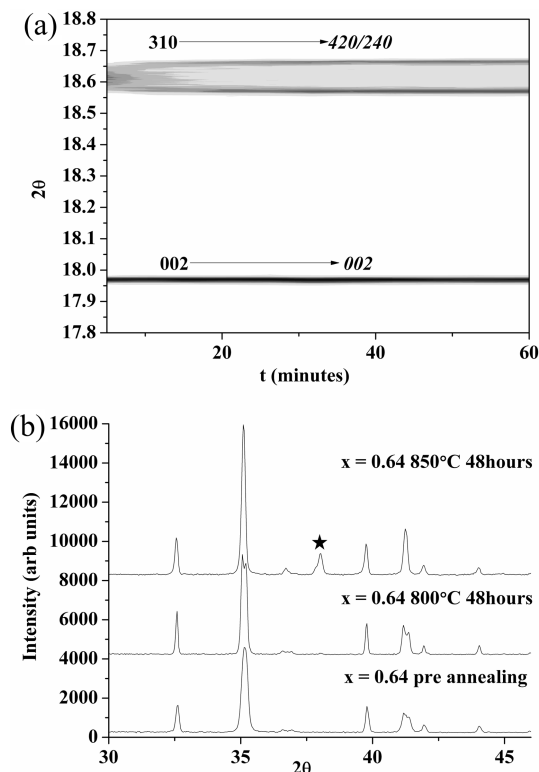(13) Macdonald, J. R. *Ann. Biomed. Eng.* **1992**, *20*, 289–305.

(a)

(b)

Figure 5. (a) LeBail fit of $La_{1.64}Sr_{0.36}Ga_3O_{7.32}$ at 600 °C using the tetragonal space group $P\bar{4}2_1m$ ($\lambda = 0.825451$ Å, $R_{wp} = 7.965\%$). (b) $La_{1.64}Sr_{0.36}Ga_3O_{7.32}$ after quenching, furnace cooling, and annealing for 12 h at 400 °C. The arrows indicate the tetragonal peaks in the pseudo-orthorhombic dominated furnace-cooled sample.

The transition at 565 °C to the O structure on cooling in $La_{1.64}Sr_{0.36}Ga_3O_{7.32}$ produces a sharp reduction in the conductivity (Figure. 8) associated with an increase in activation energy from 0.57 to 1.2 eV, and is thus assigned to the long-range ordering of the oxygen interstitial charge carriers.

The total conductivity (Figure 9) of a quenched $La_{1.64}Sr_{0.36}Ga_3O_{7.32}$ T phase pellet on heating over the 200–300 °C temperature range is approximately 2 orders of magnitude higher than that on cooling through this range after heating to 500 °C to form the ordered O phase (e.g., 1.55×10^{-4} S/cm on heating (T) against 5.5×10^{-6} S/cm cooling (O) at 300 °C), consistent with the T phase corresponding to disordered and the O phase to ordered carriers. The activation energy (0.95 eV) for the quenched metastable T $La_{1.64}Sr_{0.36}Ga_3O_{7.32}$ over 200–300 °C measured on heating (Figure 9), compares to 0.85 eV for tetragonal $La_{1.54}Sr_{0.46}Ga_3O_{7.27}$ at low temperature (250–400 °C) reported by Kuang and to 0.98 eV for the stable O phase in this temperature range. With increasing temperature, the conductivity of the virgin quenched T phase pellet remains higher than the furnace cooled mixed phase sample until approximately 400 °C, where the conductivity matches that of the furnace cooled sample. This is consistent with formation of the O phase in quenched samples (Figure 6a) within 30 min at this temperature. The conductivity on cooling post 500 °C measurement completely matched that for the furnace-cooled $La_{1.64}Sr_{0.36}Ga_3O_{7.32}$ pellet.

Figure 6. (a) Diffraction from $La_{1.64}Sr_{0.36}Ga_3O_{7.32}$ at 400 °C showing the transition from metastable T to stable O phase. T Miller indices in bold and O in italics. (b) XRD patterns of $La_{1.64}Sr_{0.36}Ga_3O_{7.32}$ before annealing, after annealing at 800 °C for 48 h, and after 850 °C for 48 h. The black star shows the formation of strontium doped lanthanum gallate (LSG) perovskite.
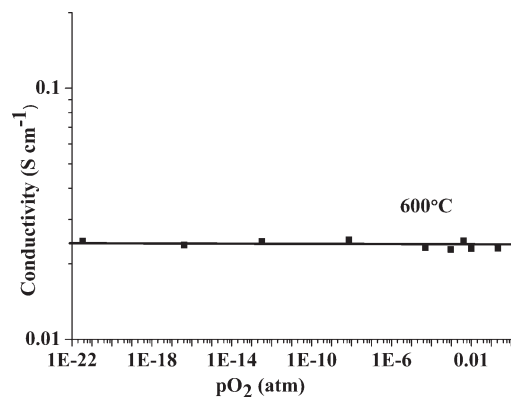

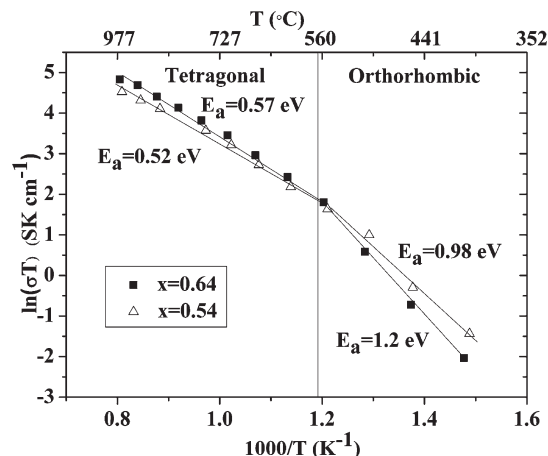**Figure 7.** p_{O_2} dependence of the total conductivity of $La_{1.64}Sr_{0.36}Ga_3O_{7.32}$ at 600 °C.

Figure 8. Conductivity of $La_{1.64}Sr_{0.36}Ga_3O_{7.32}$ (black squares, T at high temperature, O at low temperature) and $La_{1.54}Sr_{0.46}Ga_3O_{7.27}$ (triangles, T at all temperatures). The lines show the two regions with different activation energies. The postmeasurement XRD is given in SI Figure S5a.
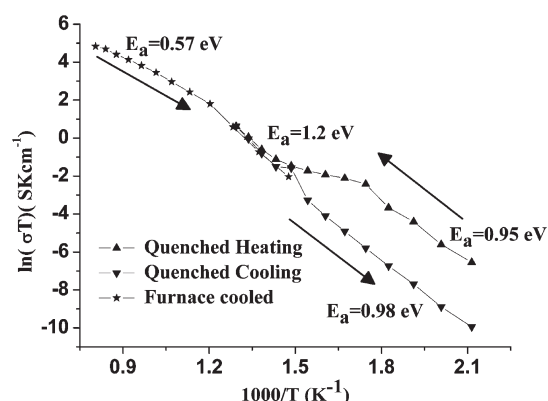

Figure 9. Conductivity of quenched $La_{1.64}Sr_{0.36}Ga_3O_{7.32}$ during thermal cycling is given by triangles. Initially the sample is tetragonal converting to orthorhombic on heating above 400 °C; on cooling, this sample retains the orthorhombic structure. The conductivity of a second sample of $La_{1.64}Sr_{0.36}Ga_3O_{7.32}$ which was furnace cooled from 1350 °C is also given for comparison and denoted by stars. This material adopts the tetragonal structure above 565 °C below which it reverts to the orthorhombic structure. Postmeasurement XRD of the furnace cooled sample (stars) is shown in SI Figure S5a; postmeasurement XRD of the quenched sample (triangles) is shown in Figure S5b.

Discussion

The total conductivity versus temperature in air for $0 \leq x \leq 0.64$ is shown in Figure 10a with $La_{0.8}Sr_{0.2}Ga_{0.83}Mg_{0.17}O_{2.815}$[14] (LSGM) for comparison. The conductivity at $x = 0.54$ is approximately 3 orders of magnitude greater than the parent material. The total conductivity of $x = 0.6$ $La_{1.6}Sr_{0.4}Ga_3O_{7.3}$ at 500 °C is 6.8×10^{-3} S/cm, which compares with 4×10^{-3} S/cm for the bulk conductivity of Mg-doped $La_{10}Si_6O_{27}$,[15] 3.2×10^{-4} S/cm for the bulk conductivity of Al-doped $La_{10}Ge_6O_{27}$,[16] 5×10^{-3} S/cm for the total conductivity of LSGM $(La_{0.8}Sr_{0.2}Ga_{0.83}Mg_{0.17}O_{2.815})$[14] and $(La_{0.83}Sr_{0.17}Ga_{0.83}Mg_{0.17}O_{2.83})$,[17] and $0.004-0.01$ S/cm for the total conductivity of $Ce_{0.9}Gd_{0.1}O_{1.95}$.[4,18,19] Above 600 °C and below 400 °C, all the interstitial-based melilites are poorer conductors than vacancy-based LSGM, but over the 400−600 °C range, the $x = 0.58$ and 0.6 compositions have slightly higher conductivity than LSGM (Figure 10a).

There is a transition (Figure 8) in the conductivity of the $x = 0.54$ material, where the T phase is long-range stable at all temperatures, at a similar temperature to that found for the electrical and long-range structural transition in

(14) Huang, K. Q.; Tichy, R. S.; Goodenough, J. B. *J. Am. Ceram. Soc.* **1998**, *81*, 2565–2575.
(15) Yoshioka, H. *Chem. Lett.* **2004**, *33*, 392–393.
(16) Leon-Reina, L.; Losilla, E. R.; Martinez-Lara, M.; Martin-Sedeno, M. C.; Bruque, S.; Nunez, P.; Sheptyakov, D. V.; Aranda, M. A. G. *Chem. Mater.* **2005**, *17*, 596–600.
(17) Dotelli, G.; Mari, C. M.; Ruffo, R.; Pelosato, R.; Sora, I. N. *Solid State Ionics* **2006**, *177*, 1991–1996.
(18) Goodenough, J. B. *Ann. Rev. Mater. Res.* **2003**, *33*, 91–128.
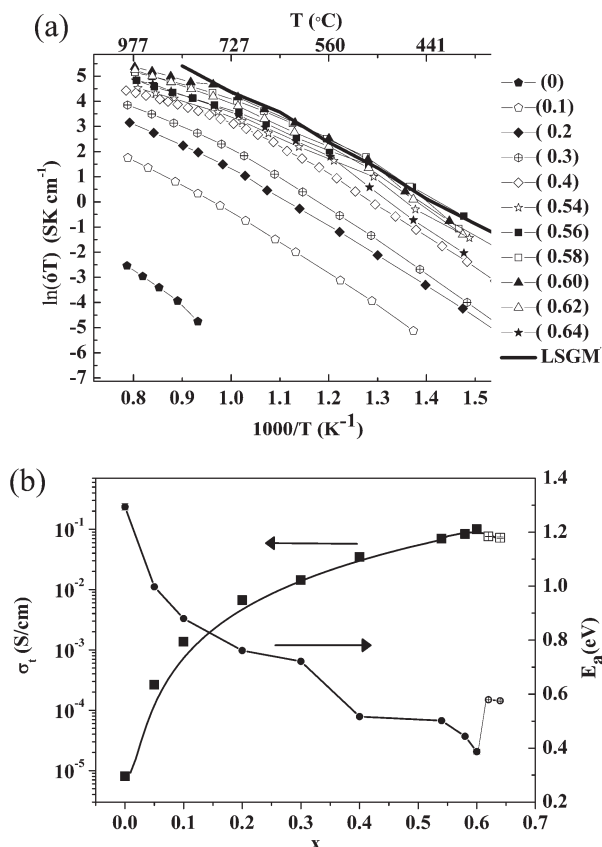(19) Zhang, T. S.; Ma, J.; Cheng, H.; Chan, S. H. *Mater. Res. Bull.* **2006**, *41*, 563–568.

(a)

(b)

Figure 10. (a) Conductivity of $La_{1+x}Sr_{1-x}Ga_3O_{7+x/2}$ where $x = 0-0.64$. LSGM is $La_{0.8}Sr_{0.2}Ga_{0.83}Mg_{0.17}O_{2.815}$.[14] (a) $x = 0.64$. The furnace cooled data in Figure 9 are the same measurement. (b) Conductivity and activation energy of $La_{1+x}Sr_{1-x}Ga_3O_{7+x/2}$ at 800 °C versus x. The low temperature stable forms are indicated by filled (T) and empty (O) symbols. The black curved line for the conductivity data is a fit to $\sigma_t = \sigma_0 + AC_{oi}^n$ where C_{oi} = number of interstials per formula unit, $\sigma_0 = 8.01 \times 10^{-6}$ S/cm, $A = 2.2(7)$, and $n = 2.7(2)$. This line is presented as a guide to the eye. The postmeasurement XRD is given in SI Figure S5a.

the ambient temperature O phase $x = 0.64$ material. The activation energy increases from 0.52 to 0.98 eV at this point- both activation energies are lower than those found at $x = 0.64$ which is O at low T. The interstitial carrier ordering which condenses into a long-range structural phase transition to the O phase beyond $x = 0.6$ thus exercises a clear influence, assigned to short-range order (SRO), on the temperature dependence of the conductivity of compositions which border the onset of the transition, suggesting that the same type of carrier association is happening at this temperature in both $x = 0.54$ and 0.64 materials but that it is short-range only at $x = 0.54$. Above the T/O structural phase transition, the more highly doped $x = 0.64$ material is more conducting, whereas below the ordering transition, the $x = 0.54$ material, which remains T with long-range carrier disorder, is more conducting. This shows the more pronounced effect of the long-range carrier ordering on the ionic transport behavior.

The variation of the conductivity with dopant concentration x is thus complicated by the effect of the long-range ordering into the O phase at high x, and the associated impact of SRO in the T phases before the structural phase transition occurs with increasing x. The total conductivity at 800 °C (Figure 10b) of $La_{1+x}Sr_{1-x}Ga_3O_{7+0.5x}$ increases as the acti-

vation energy decreases to $x = 0.6$, which is the stability limit of the T phase at room temperature. For the higher x, O phase materials, the activation energy increases and the 800 °C conductivity decreases, i.e. the materials which have the carrier ordered O structure at low temperature ($x = 0.62$ and 0.64) have a lower conductivity than $x = 0.6$ (T structure at low temperature) despite both $x = 0.62$ and 0.64 having more oxygen interstitial charge carriers. Since at 800 °C, all the compounds are T, which suggests that short-range order persists through carrier−dopant association and reduces the conductivity even in the disordered T phase for the high values of x which produce the ordered phase at low temperature. Thus, the highest conductivity is found at the stability limit of the T phase, despite the higher carrier concentration in the O phase even at O compositions above the temperature of the structural phase transition. Below 565 °C, the maximum conductivity is reached at lower x; for example at 450 °C, $x = 0.56$ (see SI Figure S6) has the highest conductivity, because the interstitial carrier order associated with the O phase reduces the large x, low temperature conductivity. Thus at all temperatures, the highest conductivities are found in materials that do not show the O structural ordering of the carriers. Carrier−dopant association associated with symmetry lowering has been observed in the isolated anion interstitial system $La_{10}(GeO_4)_{6-x}(GaO_4)_xO_{3-x/2}$ where the conductivity decreases above $x = 0.125$.[20]

The rate of increase in conductivity with x (Figure 10b) decreases as x increases, consistent with carrier ordering or mobility blocking associated with the T/O transition. This contrasts with the linear behavior observed for $(Ba_{1-x}La_x)_2In_2O_{5+x}$[21] and may be associated with short-range order that acts as a precursor to the long-range order that causes the T to O transition.

The diffusion coefficient per carrier, D, can be computed from the equation

$$D = \sigma/[(nq^2)/(kT)]$$

where n is the number of mobile species per cubic centimeter of material and q is the charge of the mobile species. In this case, the mobile species are the oxide interstitials. Figure 11a shows D over the 400−950 °C range. At 950 °C, the diffusion coefficients are of the order of $10^{-6}-10^{-5}$ cm²/s (with a maximum of 1.6×10^{-5} cm²/s at $x = 0.6$) which compares with conductivity-derived D of 1×10^{-6} cm²/s for $La_{0.9}Sr_{0.1}Ga_{0.8}Mg_{0.2}O_3$[22] (validated with tracer diffusion). The diffusion coefficient at 800 °C (Figure 11b) increases until $x = 0.6$, with a 13-fold increase from $x = 0.1$ to the maximum at 0.6. The decrease of conductivity at higher interstitial content ($x = 0.62/0.64$) correlates with the reduced diffusion coefficient and E_a increase, associated with short-range structural ordering premonitory to the O phase transition and associated blocking of the interstitial mobility. Such

(20) Kendrick, E.; Slater, P. R. *Mater. Res. Bull.* **2008**, *43*, 3627–3632.
(21) Kakinuma, K.; Yamamura, H.; Haneda, H.; Atake, T. *Solid State Ionics* **2001**, *140*, 301–306.
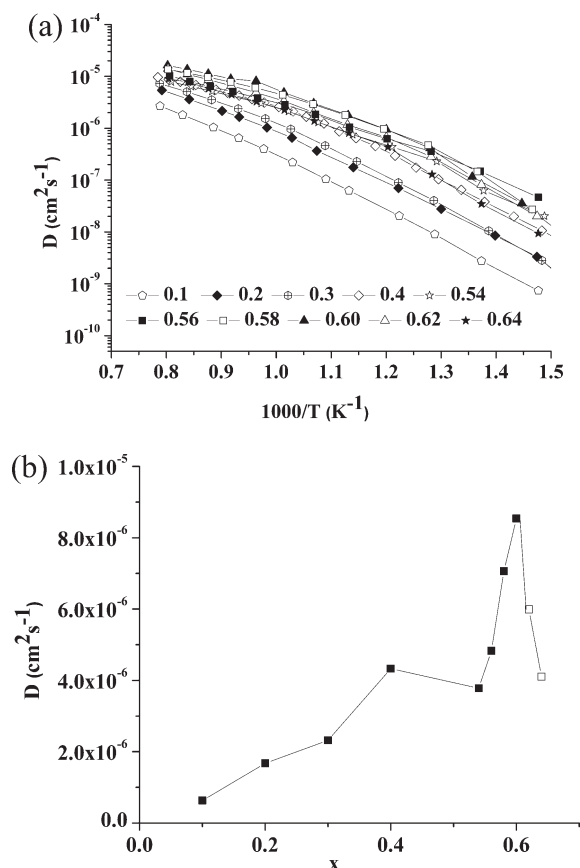(22) Ishihara, T.; Kilner, J. A.; Honda, M.; Takita, Y. *J. Am. Chem. Soc.* **1997**, *119*, 2747–2748.

(a)

(b)

Figure 11. (a) Diffusion coefficients of $La_{1+x}Sr_{1-x}Ga_3O_{7+x/2}$ ($x = 0-0.64$). (b) Diffusion coefficient versus x at 800 °C.

long-range interactions of carriers have been observed by Hohnke in $Zr(M)O_{2-x}$, $Ce(M)O_{2-x}$, and $Th(M)O_{2-x}$

($M = Sc$ and Ca).[23,24] Vacancy disordering is also known to produce a 3-fold increase in conductivity at the fluorite pyrochlore boundary in $Ln_2Zr_2O_7$.[25] In LSGM,[14] vacancy carrier trapping premonitory to long-range ordering identified in electron diffraction is proposed to impact the conductivity.

Conclusions

The solid solution range in $La_{1+x}Sr_{1-x}Ga_3O_{7+0.5x}$ extends to $x = 0.64$. The high interstitial oxide content drives a structural phase transition at $x > 0.6$ from a high temperature tetragonal phase to a low temperature O phase (< 565 °C) which strongly reduces the ionic conductivity, consistent with the transition being produced by static structural order of the interstitial charge carriers. The highest conductivities at any temperature are found in materials where the T structure is stable and interstitial order does not occur, because of the strong influence of short-range ordering associated with the T/O phase transition at temperatures above the transition and the associated effect on the temperature and dopant density dependence of the conductivity.

Supporting Information Available: Variable temperature powder X-ray diffraction data, further discussion of the impedance data, postmeasurement XRD patterns, conductivity versus x data at 450 °C, diffuse reflectance spectrum, and XRDs from annealing experiments. This materials is available free of charge via the Internet at http://pubs.acs.org.

(23) Hohnke, D. K. *J. Phys. Chem. Solids* **1980**, *41*, 777–784.
(24) Hurley, M. D.; Hohnke, D. K. *J. Phys. Chem. Solids* **1980**, *41*, 1349–1353.
(25) Yamamura, H.; Nishino, H.; Kakinuma, K.; Nomura, K. *Solid State Ionics*. **2003**, *158*, 359–365.